



High indium non-polar InGaN clusters with infrared sensitivity grown by PAMBE

Shruti Mukundan, Lokesh Mohan, Greeshma Chandan, Basanta Roul, S. B. Krupanidhi, Satish Shinde, K. K. Nanda, R. Maiti, and S. K. Ray

Citation: *AIP Advances* **5**, 037112 (2015); doi: 10.1063/1.4914842

View online: <http://dx.doi.org/10.1063/1.4914842>

View Table of Contents: <http://scitation.aip.org/content/aip/journal/adva/5/3?ver=pdfcov>

Published by the *AIP Publishing*

Articles you may be interested in

The effect of oxygen flow rate and radio frequency plasma power on cubic ZnMgO ultraviolet sensors grown by plasma-enhanced molecular beam epitaxy

Appl. Phys. Lett. **103**, 031114 (2013); 10.1063/1.4815995

Green luminescence of InGaN nanowires grown on silicon substrates by molecular beam epitaxy

J. Appl. Phys. **109**, 084336 (2011); 10.1063/1.3575323

GaNAs double-barrier quantum well infrared photodetector with the photodetection at 1.24 μm

Appl. Phys. Lett. **91**, 051102 (2007); 10.1063/1.2767185

High-quality InGaN/GaN multiple quantum wells grown on Ga-polarity GaN by plasma-assisted molecular-beam epitaxy

J. Appl. Phys. **89**, 5731 (2001); 10.1063/1.1360705

Incorporation of indium during molecular beam epitaxy of InGaN

Appl. Phys. Lett. **73**, 3232 (1998); 10.1063/1.122728



High indium non-polar InGaN clusters with infrared sensitivity grown by PAMBE

Shruti Mukundan,¹ Lokesh Mohan,¹ Greeshma Chandan,¹ Basanta Roul,^{1,2}
S. B. Krupanidhi,^{1,a} Satish Shinde,¹ K. K. Nanda,¹ R. Maiti,³ and S. K. Ray³

¹Materials Research Centre, Indian Institute of Science, Bangalore 560012, India

²Central Research Laboratory, Bharat Electronics, Bangalore 560013, India

³Department of Physics, Indian Institute of Technology, Kharagpur, India

(Received 12 November 2014; accepted 28 February 2015; published online 9 March 2015)

Studies on the optical properties of InGaN alloy of relatively higher indium content are of potential interest to understand the effect of indium content on the optical band gap of epitaxial InGaN. We report the growth of self assembled non-polar high indium clusters of $\text{In}_{0.55}\text{Ga}_{0.45}\text{N}$ over non-polar (11-20) a-plane $\text{In}_{0.17}\text{Ga}_{0.83}\text{N}$ epilayer grown on a-plane (11-20)GaN/(1-102) r-plane sapphire substrate using plasma assisted molecular beam epitaxy (PAMBE). Such structures are potential candidates for high brightness LEDs emitting in longer wavelengths. The high resolution X-ray diffraction studies revealed the formation of two distinct compositions of $\text{In}_x\text{Ga}_{1-x}\text{N}$ alloys, which were further confirmed by photoluminescence studies. A possible mechanism for the formation of such structure was postulated which was supported with the results obtained by energy dispersive X-ray analysis. The structure hence grown when investigated for photo-detecting properties, showed sensitivity to both infrared and ultraviolet radiations due to the different composition of InGaN region. © 2015 Author(s). All article content, except where otherwise noted, is licensed under a Creative Commons Attribution 3.0 Unported License. [<http://dx.doi.org/10.1063/1.4914842>]

I. INTRODUCTION

The popularity of III-nitride materials has taken up the semiconductor industry to newer applications because of their remarkable properties. In addition to having a direct and wide band gap of ~ 3.4 eV, a very fascinating property of GaN is the band gap tuning from 0.7 to 6.2 eV by alloying with Al or In. InGaN alloys of various compositions are being optimized as materials for the fabrication of light emitting diodes which are active in entire visible spectrum extending up to ultraviolet wavelengths.¹⁻³ Indium rich InGaN alloys are now being considered potential candidates for longer wavelength emitters, thermionic emitters, multi junction solar cells, etc.⁴⁻⁶ A concern with these III-nitride materials are the intrinsic and strong polarization fields resident in the lattice. To overcome such polarization effect, substrates oriented in non-polar directions i.e. (10-10) m-plane or (11-20) a-plane are used. Devices grown on these orientations are receiving a lot of focus due to this enhanced behavior;^{7,8} however, a slight compromise in terms of quality has to be made because of the large in-plane mismatch between the lattice constants, thermal expansion coefficients and elastic constants of GaN and sapphire which leads to the generation of high densities of extended defects such as threading dislocations and basal plane stacking faults at the GaN-sapphire interface.⁹⁻¹²

The large lattice constant mismatch between GaN and InN($\sim 11\%$) results in a phase separation in their solid solution which has been theoretically predicted and experimentally observed.¹³ Growth parameters such as growth temperature, growth rate and flux ratio are seen to drastically affect the indium incorporation in the bulk InGaN films. During growth of the InGaN alloys, the evaporation of indium species from the surface will be suppressed at lower temperatures and higher

^aCorresponding author. Tel.: 91-80-2360 1330; fax: +91- 80- 2360 7316 E-mail: sbk@mrc.iisc.ernet.in



growth rates as the indium species become trapped by the growing layer.^{14,15} A few attempts are reported in the literature to incorporate high indium in InGaN alloys where thin InGaN layers were grown as GaN/InGaN/GaN double heterostructures.¹⁶ First report of epitaxial growth of non-polar indium rich InGaN was on InN template on nitridated r-sapphire substrates.¹⁷ Few reports are available in the literature for the study of the non polar InGaN based multiple quantum well (MQW) structures and other devices. Song *et al.* studied the effect of periodicity of a-plane InGaN/ GaN multiple quantum wells on the output power of the LEDs grown by MOCVD.¹⁸

In our attempt to grow self assembled non-polar high indium InGaN quantum dots for the fabrication of high efficiency and bright LEDs operating in longer-wavelength regions, we have succeeded to grow non-polar high indium InGaN clusters of micron dimensions over non-polar (11-20) a-plane InGaN epilayers grown on 200nm GaN/Al₂O₃ (1-102) substrate. Detailed investigation of the structural and optical properties of the structure is undertaken in this work. Further systematic work on optimizing the growth conditions to obtain quantum confinement of the cluster is under process.

II. EXPERIMENTAL

Non-polar (11-20) a-plane InGaN epilayers were grown on 200nm GaN/Al₂O₃ (1-102) substrate using an Omicron Nanotechnology plasma assisted molecular beam epitaxy (PAMBE) system. Sapphire substrates were first degreased using trichloroethylene, etched using H₂SO₄:H₃PO₄ (3:1) at 150°C for 20 min and rinsed with deionized water before loading into the molecular-beam epitaxy chamber. Thermal cleaning was done at 850°C inside the MBE chamber for 30 min under ultra high vacuum (MBE pressure $\sim 1 \times 10^{-10}$ mbar). Growth of the a-GaN film involved a two step growth process whereby a low temperature GaN buffer layer of thickness 20 nm was grown at 500°C followed by GaN epilayer growth at 760°C. RF power and flow rate were kept constant at 350W and 0.5 sccm, respectively. A pyrometer was used to measure the substrate temperature, which was calibrated at the melting point of Al (660°C). The Ga beam equivalent pressure (BEP) was kept at 5.6×10^{-7} mbar, corresponding to the growth in the slightly nitrogen rich region. Following which, (11-20) a-plane InGaN was grown at 550°C over the GaN epilayer for 2 hours in the same chamber. Nitrogen flow rate and RF power of nitrogen plasma were kept constant at 1 sccm and 350 watt respectively. Gallium BEP was kept at 1.87×10^{-7} mbar and that of indium was at 1.17×10^{-7} mbar. The growth was continued for 1 more hour with increased indium BEP of 1.54×10^{-7} mbar to incorporate higher indium into the lattice keeping all other conditions constant.

The as-grown samples were characterized by high-resolution x-ray diffraction (HRXRD), field emission scanning electron microscopy (FESEM), Energy Dispersive Spectroscopy (EDS) and low temperature photoluminescence (PL) spectroscopy. The structural characterization of GaN films were carried out by HRXRD measurements using a double crystal four-circle diffractometer (Bruker-D8 DISCOVER) with Cu K α ($\lambda = 1.5418$ Å) radiation. To study the surface morphology and map the elements, FESEM images were obtained along with EDS mapping using FEI – 3D Quanta system. Temperature dependent PL spectra were recorded in the temperature range 10-300 K using a closed cycle optical cryostat and He-Cd laser of 325 nm excitation wavelength with a maximum input power of 30 mW. The room temperature UV and IR photodetection of the InGaN film was investigated by measuring *I-V* characteristics using computer interfaced Agilent-4155 source meter system under UV and IR light illumination, respectively. Photodetector structures were formed on the samples by standard photolithography followed by metal (Al) deposition and liftoff to create the interdigitated electrode structures with a finger spacing and finger width of 10 μ m.

III. RESULTS AND DISCUSSION

2 θ - ω HRXRD scan (Fig. 1) confirmed the growth of nonpolar a-InGaN epilayer oriented in the (11-20) direction and a-GaN epilayer oriented in the (11-20) direction on (1-102) r-plane sapphire. Two peaks corresponding to two different compositions of In_xGa_{1-x}N are seen in the zoomed inset in the graph. The peak at $2\theta = 56.645^\circ$ was assigned to (11-20) In_aGa_{1-a}N which corresponds to

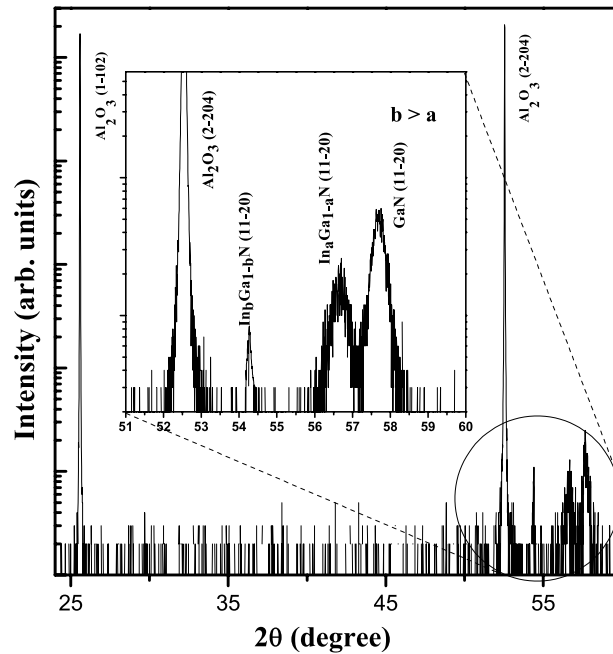


FIG. 1. HRXRD 2θ - ω scan of nonpolar (11-20) a-InGaN epilayer grown on (11-20) a-GaN/(1-102) r-plane sapphire.

the higher Ga composition, while that at $2\theta = 54.278^\circ$ was assigned to (11-20) $\text{In}_b\text{Ga}_{1-b}\text{N}$ which corresponds to the higher indium composition. The peak at $2\theta = 57.7^\circ$ is assigned to the a-plane GaN (11-20) reflection and at $2\theta = 52.56^\circ$ is assigned to (2-204) r-plane Al_2O_3 substrate. The concentration of indium in the InGaN films was determined by calculating the shift in the peak position of (11-20) plane of InGaN relative to the peak position of (11-20) plane of GaN = 57.7° and peak position of (11-20) plane of InN = 51.52° by assuming that Vegard's law is valid.^{19,20} Hence we calculated the compositions of the $\text{In}_x\text{Ga}_{1-x}\text{N}$ regions are, $\text{In}_{0.17}\text{Ga}_{0.83}\text{N}$ and $\text{In}_{0.55}\text{Ga}_{0.45}\text{N}$.

The room temperature PL spectrum of GaN films exhibits a near band edge emission (NBE) at 3.417 eV which is shown as inset in figure 2(a). The slight blue shift could be attributed to an enhanced thermal strain in the film due to the lattice mismatch of sapphire and GaN film. The temperature dependent PL spectra of the $\text{In}_x\text{Ga}_{1-x}\text{N}$ films are shown in Fig. 2(a) and 2(b). Variations of NBE with temperature for both the compositions are depicted in figure 2(c). As clearly seen, both the compositions follow different trends. PL spectra recorded above 200K showed a very weak signal for the case of $\text{In}_{0.55}\text{Ga}_{0.45}\text{N}$. This might be in account of the increase of the electron-phonon interaction which leads to a strong broadening of the PL bands. The NBE-emission spectra can be well-fitted by Varshni's equation (Eq. (1)),²¹

$$E_g(T) = E_g(0) - \frac{\alpha T^2}{(\beta + T)} \quad (1)$$

Where $E_g(T)$ is the transition energy at temperature T , $E_g(0)$ is the corresponding energy at 0K, α and β are known as Varshni's thermal coefficients and the Debye temperature respectively. For $\text{In}_{0.17}\text{Ga}_{0.83}\text{N}$, the best fit was obtained for $\alpha = 2 \times 10^{-4}$ eV/K and $\beta = 350$ K while $\text{In}_{0.55}\text{Ga}_{0.45}\text{N}$ were fitted close to the initial values $\alpha = 0.28 \times 10^{-4}$ eV/K and $\beta = 300$ K. The values of Varshni's constants are within the range of reported values.²² For $\text{In}_{0.55}\text{Ga}_{0.45}\text{N}$, the phonon energy decreases first and then increases with increasing temperature, showing an S-shaped behavior of the PL energy. Similar S-shaped behavior has been reported previously by various groups for the case of InN and $\text{In}_x\text{Ga}_{1-x}\text{N}$ quantum dots and multiple quantum wells with higher In concentration.²³⁻²⁵ Cho *et al.*²⁶ reports that InGaN-related spontaneous emission features are significantly affected by different carrier recombination dynamics which vary with temperature, because of band-tail states arising from large indium alloy fluctuations, layer thickness variations, and/or defects in the MQWs. The

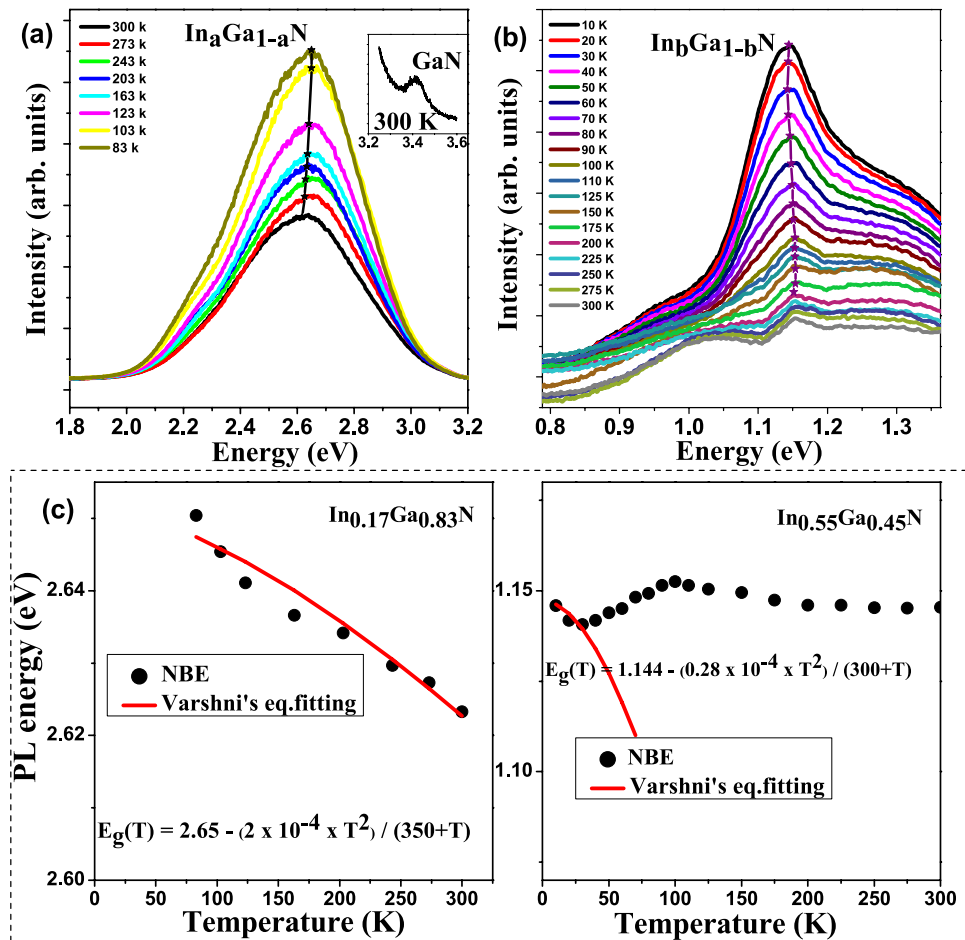


FIG. 2. Temperature dependent PL spectra of the (a) $\text{In}_a\text{Ga}_{1-a}\text{N}$ film (b) $\text{In}_b\text{Ga}_{1-b}\text{N}$ region (c) variation of NBE with temperature for both the compositions $\text{In}_{0.17}\text{Ga}_{0.83}\text{N}$ and $\text{In}_{0.55}\text{Ga}_{0.45}\text{N}$.

s-shape temperature variation of the PL energy indicates stronger localization of carrier in the high In content alloy.

Figure 3(a) shows the surface morphology of the film as seen under FESEM, randomly distributed clusters were seen over a smooth surface throughout the film. A single cluster was zoomed (Fig. 3(b)) and was found to be nearly $3\mu\text{m}$ in diameter. EDAX mapping on the same region showed the high indium content with traces of Ga (Fig. 3(c) and 3(d)) in the cluster region. Nitrogen is spread uniformly throughout the sample. Cross sectional SEM images (Fig. 3(e) and 3(f)) shows the layer of a-GaN to be ~ 185 nm in thickness while the thickness of $\text{In}_{0.17}\text{Ga}_{0.83}\text{N}$ is ~ 150 nm. The thickness of the cluster regions of higher indium content InGaN is ~ 430 nm.

The solid state miscibility gap between GaN and InN due to the large difference in interatomic spacing has been a challenge in growing $\text{In}_x\text{Ga}_{1-x}\text{N}$ alloys for long.¹³ With the observations on the morphology and composition of the film grown in this work, we postulate that during the initial growth stage, over the already grown a-GaN 200nm thick film, indium is incorporated into the lattice of GaN forming $\text{In}_{0.17}\text{Ga}_{0.83}\text{N}$ alloy which is a comparatively stable composition at the selected growth temperature. After increasing the indium flux, the excess indium atoms are segregated on top of the $\text{In}_{0.17}\text{Ga}_{0.83}\text{N}$ lattice to reduce the strain energy of the system. Under certain conditions, the sizes of the clusters can be reduced to a few nanometers and strong quantum confinement is generated. In other words, InGaN quantum dots can be formed.²⁷ These excluded indium atoms now act as nucleating sites for the formation on $\text{In}_x\text{Ga}_{1-x}\text{N}$ alloy of a higher composition of indium,

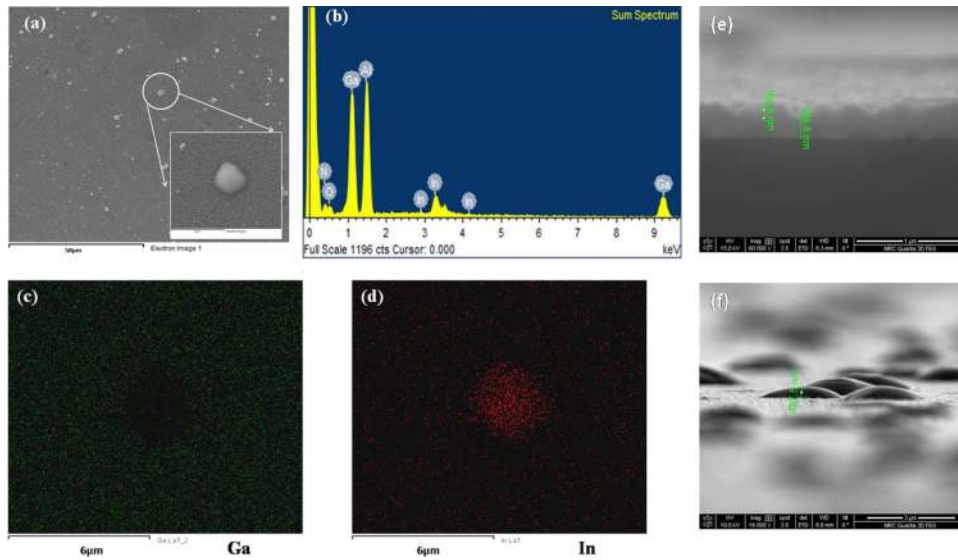


FIG. 3. (a) Surface morphology of the surface of the film as seen in FESEM with a single cluster zoomed in the inset (b) EDAX spectrum showing the elements present (c,d) mapping for tracing Ga and In by EDAX (e,f) cross sectional SEM of the sample.

which in our case turns out to be $\text{In}_{0.55}\text{Ga}_{0.45}\text{N}$. The absence of separate peaks for In and InN in XRD supports our postulated mechanism.

For a given heterogeneity of composition, the incidental non-stoichiometric regions may respond differently to the incident radiation depending on the wavelength. In order to study the photo-response of the films, photodetector structures were fabricated on the sample by standard photolithography followed by metal (Al) deposition and liftoff to create the interdigitated electrode structures with a finger spacing and finger width of $10\ \mu\text{m}$. The contacts were annealed in air at 200°C for 15 min. Fig. 4(a) shows the schematic of the device fabricated. Fig. 4(b) shows the room temperature I-V characteristic of the $\text{In}_x\text{Ga}_{1-x}\text{N}$ in dark and under IR and UV illumination.

A lamp of wavelength 360 nm with an intensity $0.3\ \text{mW}/\text{cm}^2$ was used as the UV light source for response studies. A Phillips IR lamp with a high intensity of $10\ \text{mW}/\text{cm}^2$ was used as the broadband source of IR radiation with a peak wavelength of 1000 nm. At 2V applied bias, the dark current, IR photocurrent and UV photocurrent of $\text{In}_x\text{Ga}_{1-x}\text{N}$ film were $1.26 \times 10^{-6}\ \text{A}$, $1.35 \times 10^{-6}\ \text{A}$ and $1.5 \times 10^{-6}\ \text{A}$ respectively. Responsivity (R_λ), defined as the ratio of photocurrent generated to the intensity of the incident light on the effective area of a photoconductor, was estimated using Eq. (2)

$$R_\lambda = \frac{\Delta I_\lambda}{P_\lambda S} \quad (2)$$

External quantum efficiency (EQE) is defined as the number of carriers circulating through a photodetector per absorbed photon and per unit time, and can be expressed as Eq. (3),

$$\text{EQE} = \frac{hcR_\lambda}{e\lambda} \quad (3)$$

where, ΔI_λ is the difference between the photoexcited current and dark current, P_λ is the light intensity radiated on the sample, λ is the exciting wavelength, $S = 0.01\ \text{cm}^2$ is the effective illuminated area for the device, h Planck's constant, c the velocity of light and e the electronic charge.²⁸ For an incident wavelength of 360 nm at 2V, the measured R_λ was found to be $0.082\ \text{A}/\text{W}$ for the UV illumination and for an incident wavelength of 1000 nm (broad source) at 2V, R_λ was found to be $9.57 \times 10^{-4}\ \text{A}/\text{W}$ for the IR illumination. EQE of the $\text{In}_x\text{Ga}_{1-x}\text{N}$ device showed a higher value of 28.1×10^{-2} for UV illumination as compared to under the IR illumination, which resulted

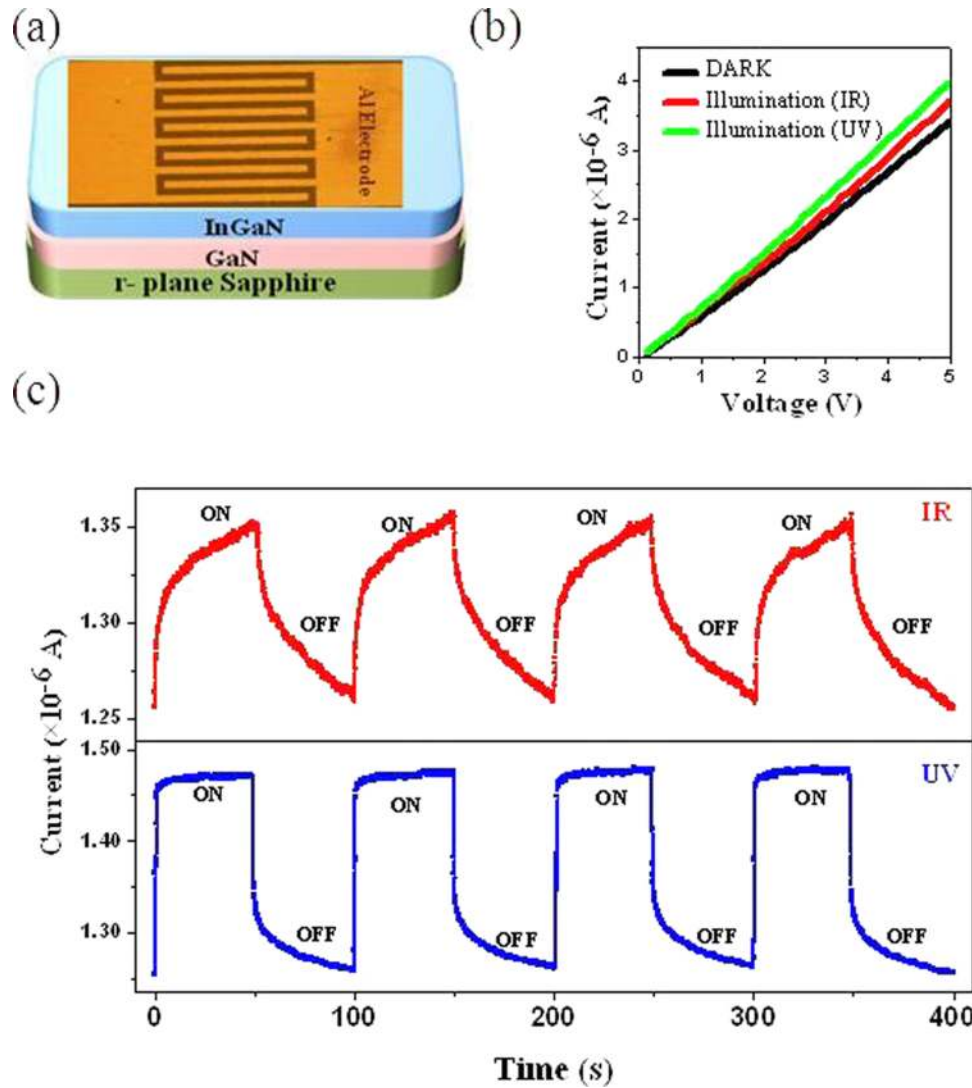


FIG. 4. (a) Schematic of the photodetector device fabricated (b) Room temperature I-V characteristic of the $\text{In}_x\text{Ga}_{1-x}\text{N}$ film in dark, under IR and UV illumination (c) Measured transit response of the fabricated photodetector at 2 V, as we switched the UV and IR excitation ON and OFF respectively.

in the EQE of 11.9×10^{-4} . As seen from HRXRD and FESEM, $\text{In}_{0.17}\text{Ga}_{0.83}\text{N}$ dominates over $\text{In}_{0.55}\text{Ga}_{0.45}\text{N}$ and is sensitive to UV radiation and hence such observation.

The reason for the slow photo response of the device is the high threading dislocations and basal stacking faults.²⁹ For comparing the performance of the device, similar photodetector structure was fabricated on bare a-GaN epilayer. The device showed no response to IR radiation but it showed UV sensitivity. At 2V applied bias, the dark current and UV photocurrent of a-GaN film were 1.9×10^{-6} A and 2.37×10^{-6} A respectively. For an incident wavelength of 360 nm at 2V, the measured R_λ was found to be 0.157 A/W for the UV illumination. EQE of the device was found to be 53.94×10^{-2} . Thus, introducing InGaN layer over the GaN film has negatively affected the device performance in the UV rays because of the introduction of higher defect levels at the interface. The advantage of this structure is the sensitivity to different wavelength of incident light.

Figure 4(c) shows the measured transit response of the fabricated device at 2 V, as we switched the UV and IR excitation on and off respectively. The dynamic response of the device was recorded for 4 on/off cycles and it displayed a rather stable response.

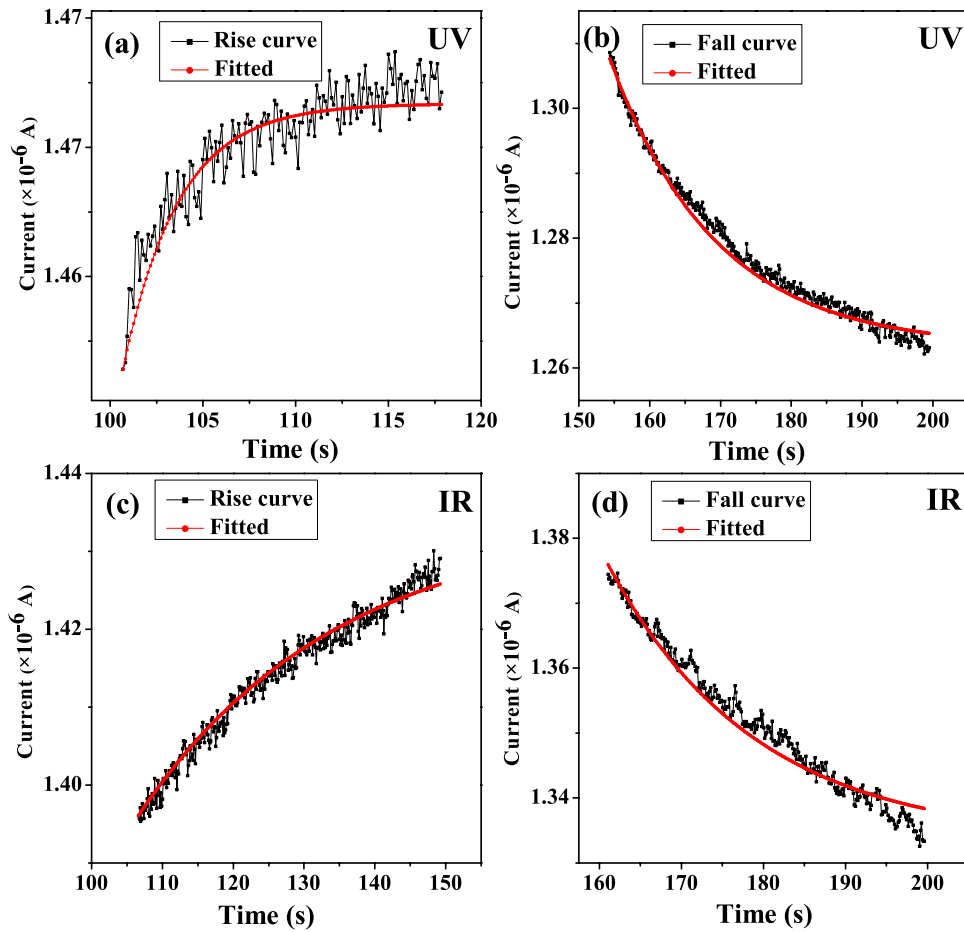


FIG. 5. Time response of photocurrent of the $\text{In}_x\text{Ga}_{1-x}\text{N}$ film under UV illumination during (a) rise time (b) fall time and under IR illumination during (c) rise time and (d) fall time.

To quantify the response time of the rise and fall of the photocurrent in the InGaN film, Eqs. (4) and (5) were used,³⁰

$$\text{Rise curve: } I(t) = I_{\text{dark}} + A \left[1 - \exp \left\{ \frac{-(t - t_0)}{\tau} \right\} \right] \quad (4)$$

$$\text{Fall curve: } I(t) = I_{\text{dark}} + A \exp \left\{ \frac{-(t - t_0)}{\tau} \right\} \quad (5)$$

where I_{dark} is the dark current, A is the scaling constant, τ is the time constant and t_0 is the time when light source was switched on or off. The time constant was estimated by fitting Eqs. (4) and (5) to the experimental time response of photocurrent during rise and fall as shown in Fig. 5(a) and 5(b) under UV illumination and in Fig. 5(c) and 5(d) under IR illumination. The values of rise time and fall time were found to be 3 s and 15 s respectively under UV illumination while they were found to be 28 s and 18 s respectively with IR illumination. UV response time calculated for a bare a-GaN film were found to be rise time = 6 s and fall time = 15 s. Slower rise time for the InGaN film is due to smaller band gap while the same value of fall time suggest similar levels of defect densities in the GaN and InGaN film. The significance of these time constants is that it suggests the presence of the defect levels in the sample. $\text{In}_{0.55}\text{Ga}_{0.45}\text{N}$ being sensitive to IR radiation is observed to take longer time to respond to the corresponding illumination. The formation of $\text{In}_{0.55}\text{Ga}_{0.45}\text{N}$

is postulated to be a result of the randomly segregated indium atoms acting as nucleating centers; hence the lack of crystalline quality in this composition resulting in the slow response time is justified.

IV. CONCLUSION

In summary, we have successfully grown regions of $\text{In}_{0.55}\text{Ga}_{0.45}\text{N}$ with high indium content over a uniform $\text{In}_{0.17}\text{Ga}_{0.83}\text{N}$ epilayer in the process of making a high bright LED structure. To assess the quality of photo response, we have fabricated a photo detector which exhibited sensitivity to both UV and IR radiations. Variation of NBE with temperature for both the InGaN compositions were plotted and fitted with Varshni's equation. For $\text{In}_{0.17}\text{Ga}_{0.83}\text{N}$, the best fit was obtained for $\alpha = 2 \times 10^{-4}$ eV/K and $\beta = 350$ K while for $\text{In}_{0.55}\text{Ga}_{0.45}\text{N}$, fitted close to the initial values $\alpha = 0.28 \times 10^{-4}$ eV/K and $\beta = 300$ K. For $\text{In}_{0.55}\text{Ga}_{0.45}\text{N}$, the phonon energy decreases first, but then increases with increasing temperature, showing an S-shaped behavior of the PL energy. A simple mechanism for the formation of such multi-compositional InGaN film is postulated. The multi-compositional film when fabricated into a photodetector, could detect both IR and UV radiation. EQE in case of UV illumination and IR illumination was found to be 28.1×10^{-2} and 11.9×10^{-4} respectively. The value of rise time and fall time was found to be 3 s and 15 s respectively when under UV illumination while they were 28 s and 18 s respectively when under IR illumination. Further work is in progress to optimize the size of the clusters and to achieve quantum confinement.

ACKNOWLEDGMENTS

The authors are thankful to the Council of Scientific and Industrial Research (CSIR) India, and Indian Institute of Science (IISc) and Department of Information Technology (DIT) for providing the financial support.

- ¹ R. C. Powell, N.E. Lee, and J. E. Greene, *Appl. Phys. Lett.* **60**, 2505 (1992).
- ² F.A. Ponce and D.P. Bour, *Nature* **386**, 351 (1997).
- ³ S. Nakamura, *Jpn. J. Appl. Phys.* **30**, 1705 (1991).
- ⁴ B. N. Pantha, R. Dahal, J. Li, J. Y. Lin, H. X. Jiang, and G. Pomrenke, *Appl. Phys. Lett.* **92**, 042112 (2008).
- ⁵ D. V. P. McLaughlin and J. M. Pearce, *Metall. Mater. Trans. A* **44**, 1947 (2013).
- ⁶ W. Junqiao, *J. Appl. Phys.* **106**, 011101 (2009).
- ⁷ E.Y. Lin, C.Y. Chen, T.S. Lay, Z.X. Peng, T.Y. Lin, T.C. Wang, and J.D. Tsay, *Physica B* **405**, 1857–1860 (2010).
- ⁸ Theeradetch Detchprohm, Mingwei Zhu, Yufeng Li, Yong Xia, Christian Wetzel, Edward A. Preble, Lianghong Liu, Tanya Paskova, and Drew Hanser, *Appl. Phys. Lett.* **92**, 241109 (2008).
- ⁹ F. Bernardini, V. Fiorentini, and D. Vanderbilt, *Phys. Rev. B* **56**, R 10 024 (1997).
- ¹⁰ M. Stutzmann, O. Ambacher, M. Eickhoff, U. Karrer, A. Lima Pimenta, R. Neuberger, J. Schalvig, R. Dimitrov, P. J. Schuck, and R. D. Grober, *Phys. Status Solidi B* **228**, 505 (2001).
- ¹¹ T. J. Badcock, M. J. Kappers, M. A. Moram, R. Hao, P. Dawson, and C. J. Humphreys, *Phys. Status Solidi B* **249**(3), 494–497 (2012).
- ¹² Mohana K. Rajpalke, BasantaRoul Mahesh Kumar, Thirumaleshwara N. Bhat, Neeraj Sinha, and S.B. Krupanidhia, *ScriptaMaterialia* **65**, 33-36 (2011).
- ¹³ S. Yu. Karpov, *MRS Internet Journal of Nitride Semiconductor Research* **3**, pp. e16 (1988).
- ¹⁴ S. Keller, B.P. Keller, D. Kapolnek, A.C. Abare, H. Masui, L.A. Coldren, U.K. Mishra, and S.P. Den Baars, *Appl. Phys. Lett.* **68**, 3147 (1996).
- ¹⁵ S. Keller, B.P. Keller, D. Kapolnek, S.P. Den Baars, I.K. Shmagin, R.M. Kolbas, and S. Krishnankutty, *J. Cryst. Growth* **170**, 349 (1997).
- ¹⁶ R. Singh, D. Doppalapudi, T. D. Moustakas, and L. T. Romano, *Appl. Phys. Lett.* **70**, 1089 (1997).
- ¹⁷ M. Noda, Y. Kumagai, S. Takado, D. Muto, H. Na, H. Naoi, T. Araki, and Y. Nanishi, *Phys. Status Solidi (C)* **4**(7), 2560–2563 (2007).
- ¹⁸ Keun Man Song, Jong-Min Kim, Chan-Soo Shin, Sung-Min Hwang, and Dae-Ho Yoon, *Semicond. Sci. Technol.* **27**, 015011 (2012).
- ¹⁹ N.A. El-Masry, E.L. Piner, S.X. Liu, and S.M. Bedair, *Appl. Phys. Lett.* **72**, 40 (1998).
- ²⁰ R. Singh, D. Doppalapudi, T.D. Moustakas, and L.T. Romano, *Appl. Phys. Lett.* **70**, 1089 (1997).
- ²¹ Y. P. Varshni, *Physica (Utrecht)* **34**, 149 (1967).
- ²² M. Leroux, N. Grandjean, B. Beaumont, G. Nataf, F. Semond, J. Massies, and P. Gilbert, *J. Appl. Phys.* **86**, 3721 (1996).
- ²³ J.S. Huang, Z. Chena, X.D. Luo, Z.Y. Xua, and W.K. Ge, *J. Cryst. Growth* **260**, 13–17 (2004).

- ²⁴ Q Li, S J Xu, M H Xie, and S Y Tong, *J. Phys. Condense Matter* **17**, 4853–4858 (2005).
- ²⁵ F. B. Naranjo, M. A. Sánchez-García, F. Calle, and E. Calleja, *Appl. Phys. Lett.* **80**(2), (2002).
- ²⁶ Yong-Hoon Cho, G. H. Gainer, A. J. Fischer, J. J. Song, S. Keller, U. K. Mishra, and S. P. Den Baars, *Appl. Phys. Lett.* **73**, 1370 (1998).
- ²⁷ Tongtong Zhu, Fabrice Oehler, Benjamin P. L. Reid, Robert M. Emery, Robert A. Taylor, Menno J. Kappers, and Rachel A. Oliver, *Appl. Phys. Lett.* **102**, 251905 (2013).
- ²⁸ LinfengHu, Jian Yan, Meiyong Liao, Limin Wu, and Xiaosheng Fang, *Small*. **7**(8), 1012–1017 (2011).
- ²⁹ D. Kundys, S. Schulz, F. Oehler, D. Sutherland, T. J. Badcock, P. Dawson, M. J. Kappers, R. A. Oliver, and C. J. Humphreys, *Journal of Applied Physics* **115**, 113106 (2014).
- ³⁰ S. Ghosh, B. K. Sarker, A. Chunder, L. Zhai, and S. I. Khondaker, *Appl. Phys. Lett.* **96**, 163109 (2010).